Photoelectrocatalytic inactivation of *Pseudomonas aeruginosa* using an Ag-decorated TiO_2 photoanode

Ruth Belinda Domínguez-Espíndola [a], Carmina Bruguera-Casamada [b], Susana Silva-Martínez [c,**], Rosa María Araujo [b], Enric Brillas [d], Ignasi Sirés [d,*]

[a] *Department of Chemistry, Curtin University, Bentley, Western Australia 6102, Australia*

[b] *Sec. Microbiologia, Virologia i Biotecnologia, Departament de Genetica, Microbiologia i Estadística. Facultat de Biologia, Universitat de Barcelona, Avinguda Diagonal 643, 08028 Barcelona, Spain*

[c] *Centro de Investigaciones en Ingeniería y Ciencias Aplicadas, Universidad Autónoma del Estado de Morelos, Cuernavaca, Mexico*

[d] *Laboratori d'Electroquímica dels Materials i del Medi Ambient, Departament de Química Física, Facultat de Química, Universitat de Barcelona, Martí i Franquès 1-11, 08028 Barcelona, Spain*

Corresponding author: * i.sires@ub.edu (I. Sirés)

** ssilva@uaem.mx (S. Silva-Martínez)

Abstract

Fast and total inactivation of Gram-negative *Pseudomonas aeruginosa* in suspensions at natural pH 5.9 has been achieved by photoelectrocatalyisis (PEC), using Ag-decorated TiO_2 photoanodes onto transparent conducting indium tin oxide (ITO) under UVA irradiation. The assays were made with 100 mL of bacterial suspensions in an undivided cell equipped with a photoanode, a stainless steel cathode and Ag|AgCl (3 M KCl) as reference electrode. Total inactivation was obtained in only 5 min using coatings with 4 wt.% Ag, 25 mM Na_2SO_4 as the electrolyte and 1.70 V as applied bias potential. Comparative photocatalytic treatments reached total inactivation at much longer time, suggesting the crucial role of hydroxyl radicals in PEC. These oxidants, which were detected by electron spin resonance, attacked the outer cell wall very effectively, since the recombination of the electron/hole pairs photoinduced under UVA irradiation was reduced. As characterized by high-resolution transmission electron microscopy (HRTEM), the best synthesized Ag-TiO_2 thin-film photoanode mainly contains anatase TiO_2 nanopowder decorated with Ag nanoparticles of ca. 45 nm. Analyses by X-ray powder diffraction and UV/Vis spectroscopy were also performed. The potential use of PEC for bacterial disinfection was confirmed for the rod-shaped Gram-positive *Bacillus atrophaeus*, which was more slowly inactivated due to its different cell wall structure. Scanning electron micrographs of both bacteria showed that PEC induced a high roughness, cell lysis and accumulation of cellular debris.

Keywords: *Bacillus atrophaeus*; Bacterial inactivation; Photoelectrocatalysis; *Pseudomonas aeruginosa*; Water disinfection

1. Introduction

Recently developed electrochemical advanced oxidation processes (EAOPs) like electrochemical oxidation (EO), electro-Fenton, UV- or solar-assisted photoelectro-Fenton and photoelectrocatalysis (PEC) have shown their great potential for water decontamination and disinfection [1-8]. The destruction of suspended or attached biofilms of pathogenic bacteria is a crucial need in drinking water production, swimming pools, washing in food processing, water distribution or ballast water management [9]. Ozone, chlorine dioxide and chlorine are typically utilized for water disinfection. However, they can yield hazardous products, including haloacetic acids and trihalomethanes [1]. To overcome these drawbacks, non-toxic antibacterial nanostructures have been proposed [10,11]. EAOPs also represent an alternative for bacterial inactivation, since they are eco-friendly methods based on the generation of reactive oxygen species (ROS) like the hydroxyl radical ($^{\bullet}OH$), which is able to react with cell membrane components causing lysis and the death of bacteria [1,12,13].

PEC is electrochemically-assisted photocatalysis (PC) [14]. PC consists in the photoexcitation of an electron from the valence band (VB) of a semiconductor to the conduction band (CB, e^-_{CB}), with production of a positively charged vacancy or hole (h^+_{VB}) from reaction (1) [14-18]. The photogenerated holes can oxidize organic molecules or react with water to form the $^{\bullet}OH$ via reaction (2). The photoinduced electrons can produce other ROS like superoxide radical anion ($O_2^{\bullet-}$), hydroperoxyl radical ($HO_2^{\bullet}$) and H_2O_2 from reactions (3)-(6).

$$\text{Semiconductor} + h\nu \rightarrow e^-_{CB} + h^+_{VB} \quad (1)$$

$$h^+_{VB} + H_2O \rightarrow {}^{\bullet}OH + H^+ \quad (2)$$

$$e^-_{CB} + O_2 \rightarrow O_2^{\bullet-} \quad (3)$$

$$O_2^{\bullet-} + H^+ \rightarrow HO_2^{\bullet} \quad (4)$$

$$2\,HO_2^{\bullet} \rightarrow H_2O_2 + O_2 \quad (5)$$

$$H_2O_2 + O_2^{\bullet-} \rightarrow {}^{\bullet}OH + OH^- + O_2 \quad (6)$$

The main drawback of PC is the fast recombination of the e^-_{CB}/h^+_{VB} pairs, which causes a great efficiency loss. This is solved in PEC by applying either a constant current density (j) or a constant bias anodic potential (E_{bias}) to the illuminated semiconductor. This allows the continuous extraction of the e^-_{CB} from the anode through the external electrical circuit, thus inhibiting reactions (3)-(6) and recombination. Hence, a higher effective accumulation of holes and $^{\bullet}OH$ from reactions (1) and (2) is feasible, leading to much higher overall efficiency than PC [14,17].

The best semiconductor for PC and PEC is TiO_2 because it is non-toxic, highly stable against photocorrosion and inexpensive. It is typically utilized as a mixture of two nanocrystalline forms, namely anatase and rutile, needing UV light to photoexcite the electrons from their VB since their bandgap (E_{bg}) is 3.0-3.2 eV [17]. TiO_2 thin layers from powders can be prepared by several procedures including sol-gel [14,19], microwave-assisted dip-coating [20], chemical vapor deposition [14] or electrophoretic deposition [21-23]. Ti, indium tin oxide (ITO) and fluorinated tin oxide (FTO) are widely used as substrates.

The photocatalytic efficiency of TiO_2 thin films in practice is limited by the small UV fraction (~ 5%) of the solar spectrum [24]. Lately, three main strategies have been followed to improve the oxidation power of this semiconductor in PEC [14,17]: (i) use of nanostructured TiO_2 materials like nanotube bundles or arrays, nanobelts, nanowires or nanorods, showing large effective area that allows greater light absorption; (ii) band-gap engineering to absorb visible light, based on TiO_2 doping to substitute O atoms either with transition metal ions like Cr, Co, W, Zr and Fe or with non-metals like N, F,

S, B and C; and (iii) surface decoration with noble metal nanoparticles like Ag, Pd or Au to act as electron trap of photoinduced electrons. In the case of Ag-TiO_2, Ag promotes the charge transfer at the interface with TiO_2, minimizing the e^-_{CB}/h^+_{VB} recombination [17,18]. Furthermore, the surface plasmon resonance of Ag nanoparticles enhances the visible light response of the photocatalyst [25]. The use of Ag-TiO_2 for PEC disinfection is particularly interesting because of the high antibacterial activity and biocompatibility of Ag [26-28].

The decoration of semiconductors with Ag particles is carried out by dipping the substrate into an Ag^+ solution, followed by exposure to UV radiation to induce Ag^+ photoreduction [28-33]. The efficient photocatalytic power of Ag-TiO_2 films for the degradation of 10 mg L^{-1} phenol solutions at pH 3.0 has been reported using UV light [34] and sunlight [35]. Recently, several authors have described the inactivation of different bacteria by PC under UV and solar irradiation using Ag-TiO_2 [36-38]. Ag-TiO_2 photoanodes have also been studied for PEC inactivation of *Escherichia coli* and *Staphylococcus aureus* [39], *Mycobacterium smegmatis* [28] and *Mycobacterium kansasii* and *Mycobacterium avium* [40], showing the superiority of the decorated photoanodes.

Pseudomonas aeruginosa is a rod-shaped Gram-negative bacterium, ubiquitous in soil and water as well as in animals and in plants [12]. This aerobic pathogen can cause mild to severe infections such as pneumonia, dermatitis, keratitis, otitis and nosocomial infections [41]. The increasing antibiotic resistance of such bacteria makes necessary the use of efficient methods to ensure a fast inactivation in water. Nouri et al. [11] reported the mortality of 99% of 5.6×10^{13} CFU mL^{-1} of *P. aeruginosa* using chitosan films loaded with 3% mormollite/CuO nanocomposite. Hussain et al. [42] showed complete disinfection of water with 1.8×10^9 CFU mL^{-1} in 0.3% NaCl at pH 7 after 20

114 min of adsorption onto a graphite intercalation compound. Inactivation of about 99%
115 was also found by electrolyzing 10^8 CFU mL^{-1} of *P. aeruginosa* with a stainless steel
116 anode at j = 70 μA cm^{-2} for 1 h [43]. Additionally, the effectiveness of •OH has been
117 well proven by means of Fenton process with ferrocene-loaded polymeric micellar
118 nanoplatforms [10], EO with boron-doped diamond (BDD) and dimensionally stable
119 anodes [44], and PC with Ag-TiO_2 microspheres under UVC illumination [36].
120 The aim of this work is to study the inactivation of *P. aeruginosa* by UVA-assisted
121 PEC with Ag-decorated TiO_2 deposited onto ITO. The influence of the percentage of
122 Ag loading, supporting electrolyte content and E_{bias} on the disinfection process was
123 examined. Comparative treatment by PC was made to show the advantages of PEC. The
124 production of •OH was confirmed by electron paramagnetic resonance (EPR). The
125 characteristics of the best Ag-TiO_2 photoelectrode were ascertained by high-resolution
126 transmission electron microscopy (HRTEM), energy dispersive X-ray analysis (EDX),
127 X-ray powder diffraction (XRD) and UV/Vis spectroscopy. The study was extended to
128 the Gram-positive bacterium *Bacillus atrophaeus* to show the performance of the
129 photoanode against other kinds of cell walls. The changes in bacterial morphology were
130 analyzed by scanning electron microscopy (SEM).

131 **2. Materials and methods**

132 *2.1. Chemicals*

133 Sodium sulfate used as supporting electrolyte was of analytical grade purchased
134 from Panreac Química. Reagents used for the preparation of the photoanodes, bacterial
135 culture and all the analysis were of analytical grade purchased from Panreac Química,
136 Merck, Fluka and Sigma-Aldrich. Solutions were prepared with ultrapure water from a
137 Millipore Milli-Q system (resistivity > 18.2 MΩ cm).

2.2. Preparation of the Ag-TiO_2 photoanodes

First, TiO_2 nanoparticles were deposited onto ITO glass substrates purchased from MSE Supplies (25 mm × 50 mm, 1.1 mm thickness, 10 Ω sq^{-1}), which were electrochemically cleaned and then introduced as the cathode in a conventional electrophoretic cell equipped with a boron-doped diamond (BDD) anode placed in parallel at an interelectrode distance of 1.0 cm. The back side of the ITO was conveniently isolated to prevent any deposition. The cell was filled with 30 mL of a suspension of 1.5 g TiO_2 P-25 (80% anatase, 20% rutile, average particle diameter of 20 nm) purchased from Degussa in 5% (v/v) isopropanol/water, after 15 min of sonication. TiO_2 deposition was performed by applying a cell voltage of 4 V for only 60 s at ambient temperature. The resulting ITO/TiO_2 thin film was subsequently annealed at 450 ºC for 30 min. The deposition / annealing cycle was made four times in order to ensure the formation of a compact layer of TiO_2 with good adherence and crystallinity. A sketch of the setup use for the preparation of ITO/TiO_2 is shown in Fig. S1a.

The decoration of the above ITO/TiO_2 material with Ag was performed using a solution containing 27.5 mL isopropanol, 0.8 mL Milli-Q water, 0.4 mL HNO_3 and either 0.0153 or 0.0612 g $AgNO_3$ (Sigma-Aldrich) to obtain photoanodes with 1% or 4% (w/w) Ag, respectively. The ITO/TiO_2 was immersed into the corresponding solution for 16 h at ambient temperature in the dark, dried at ambient temperature for 15 min and then irradiated with a 125 W UVC light bulb (λ_{max} = 254 nm) for 90 min to photoreduce the adsorbed Ag^+ ion to Ag (see Fig. S1b). Homogeneous and stable Ag-TiO_2 thin-film photoelectrodes of purple color were obtained after annealing at 450 ºC for 30 min.

2.3. Bacteria and culture

The inactivation of the rod-shaped Gram-negative bacterium *P. aeruginosa* ATCC 15442 and Gram-positive bacterium *B. atrophaeus* ATCC 9372 (previously named *B. subtilis*) was studied. The strains of both bacteria were cultured in Trypticasein Soy Agar (TSA) plates, supplied by Laboratorio Conda, at 37 ºC for 24 h. After that, each microorganism was spiked into 2 mL of 7 mM Na_2SO_4, followed by centrifugation at 14,000 rpm for 2 min and washing with 1 mL (3 times) of the same electrolyte. The final pellet was resuspended in 1 mL of 7 mM Na_2SO_4, yielding an optical density at 600 nm (O.D. 600) of 0.7±0.1, corresponding to about 10^8 CFU mL^{-1}.

2.4. Inactivation experiments

The disinfection assays by PEC were carried out in a conventional cylindrical three-electrode cell of Schott Duran® glass of 150 mL capacity. Thermostated water was recirculated through a jacket surrounding the cell to keep the suspension temperature at 25 ºC. The anode was a 3 cm^2 Ag-TiO_2 thin-film photoelectrode synthesized as described above, the cathode was a Pt spiral and the reference electrode was Ag|AgCl (3 M KCl). The back side of the coated ITO substrate was illuminated with an Omnilux 125 W UVA light bulb (λ_{max} = 360 nm), placed in parallel at a distance of 6 cm. An Amel 2053 potentiostat-galvanostat was used to provide a bias potential (E_{bias}) to the photoanode *vs*. the reference electrode. A scheme is shown in Fig. S2. For comparison, PC assays were performed under the same experimental conditions, with the prepared Ag-TiO_2 photoelectrode acting as photocatalyst, but without applying a bias potential.

The trials were carried out with 100 mL of aqueous solutions containing 7 or 25 mM Na_2SO_4 at natural pH 5.9, always under vigorous stirring at 700 rpm with a magnetic PTFE stirring bar. Each sulfate solution was spiked with a 10^8 CFU mL^{-1} of *P. aeruginosa* or *B. atrophaeus* to obtain a bacterial suspension with 10^6 CFU mL^{-1}. Before each assay, the cell was cleaned with a H_2O_2:H_2SO_4 mixture (30:70 v/v) for 10

187 min, rinsed with Milli-Q water and dried in an oven at 80 ºC. After usage, the electrodes
188 were immersed in ultrapure water at 100 °C for 10 min and finally, air dried.

189 *2.5. Analytical procedures*

190 The pH and O.D. 600 of the bacterial suspensions were measured with a Crison
191 GLP 22 pH-meter and a Camspec M108 spectrophotometer, respectively.

192 To assess the inactivation of *P. aeruginosa* and *B. atrophaeus* suspensions, 1-mL
193 samples were withdrawn at different times for 45 min of treatment as maximal. They
194 were diluted in 7 mM Na_2SO_4, cultured in duplicate on TSA plates and incubated at 37
195 ºC for 24 h. The percentage of inactivation was calculated as follows:

196 $$\% \text{ Inactivation } = \frac{N_0 - N_t}{N_0} (100) \quad (7)$$

197 where N_0 is the initial CFU value and N_t is its content at time *t*. The theoretical detection
198 limit was 1 bacterium per mL. All the trials were made in triplicate and average values
199 of percentage of inactivation are shown in figures, along with the error bars associated
200 to a 95% confidence interval.

201 The morphological features of each microorganism before and after the inactivation
202 trials were analyzed by SEM using a JEOL JSM-7001F system at 15 kV [12]. To do
203 this, each bacterial suspension was filtered through a 0.2 µm polycarbonate membrane
204 filter purchased from Millipore. The filter was immersed in a 2.5% glutaraldehyde and
205 0.1 M cacodylate solution at pH 7.4 for 30 min and further, it was post-fixed in 1%
206 OsO_4, washed with 0.2 M sodium cacodylate, dehydrated with a graded series of
207 ethanol solutions from 30% to 100% and dried. The final samples were coated with gold
208 to carry out the observation by SEM.

209 The morphological characteristics and surface composition of the raw TiO_2 and the
210 synthesized Ag(4%)-TiO_2 materials were examined by HRTEM and EDX. The latter

was powder scratched from the thin-film photoelectrode surface. Both powders were ultrasonically dispersed in isopropyl alcohol and supported on holey carbon-coated copper grids. These analyses were performed with a JEOL JEM-2100 LaB6 transmission electron microscope at 200 kV, and the EDX spectra were acquired using an INCA X-sight analyzer (Oxford Instruments) with Microanalysis Suite version 4.09 software. The crystal structure of the photoelectrode was analyzed by XRD with a PANalytical X'Pert PRO MPD Alpha1 powder diffractometer in Bragg-Brentano $\theta/2\theta$ geometry with 240 mm radius, using Cu $K\alpha_1$ radiation (λ = 1.5406 Å). The reference XRD patterns were selected from ICDD database.

The absorbance of the ITO substrate, the ITO/TiO_2 material and the Ag-TiO_2 thin-film photoelectrodes in the UV/Vis region was determined by UV/Vis spectroscopy using a Shimadzu UV-1800 UV/Vis spectrophotometer.

The generation of hydroxyl radicals under PEC conditions was confirmed by spin trapping from the analysis of its adduct with 5,5-dimethyl-1-pyrroline-*N*-oxide (DMPO) by EPR [45]. This was made by treating 10 mL of a 9.2 mM DMPO solution with 25 mM Na_2SO_4 at pH 5.9 in a three-electrode cell with a 1 cm^2 Ag(4%)-TiO_2 photoanode under 125 W UVA illumination and a 1 cm^2 stainless steel spiral cathode, with vigorous stirring provided by a magnetic PTFE bar at ambient temperature. An E_{bias} = 1.70 V vs. Ag|AgCl (3 M KCl) was applied for 15 min. The EPR analysis of the resulting solution was performed with a Bruker ESP300E spectrometer, using Win-EPR and SimFonia 2.3 software.

3. Results and discussion

3.1. Inactivation of Pseudomonas aeruginosa

A set of trials was made to assess the influence of the Ag content in the photoanode, the supporting electrolyte and the E_{bias} applied on the photoelectrocatalytic

inactivation of *P. aeruginosa*. The initial pH of 5.9 remained practically unchanged during the trials due to the low current flowing through the electrical circuit and the short electrolysis times utilized.

Fig. 1 depicts an evident enhancement of the inactivation rate as the amount of Ag decorating the TiO_2 deposit onto the ITO substrate was increased. As can be seen, for an Ag(1%)-TiO_2 photoanode in 25 mM Na_2SO_4 at E_{bias} = 1.70 V, complete disinfection was reached after 15 min of PEC (filled square), whereas only 5 min (filled triangle) were required when an Ag(4%)-TiO_2 photoanode film was used instead under similar conditions.

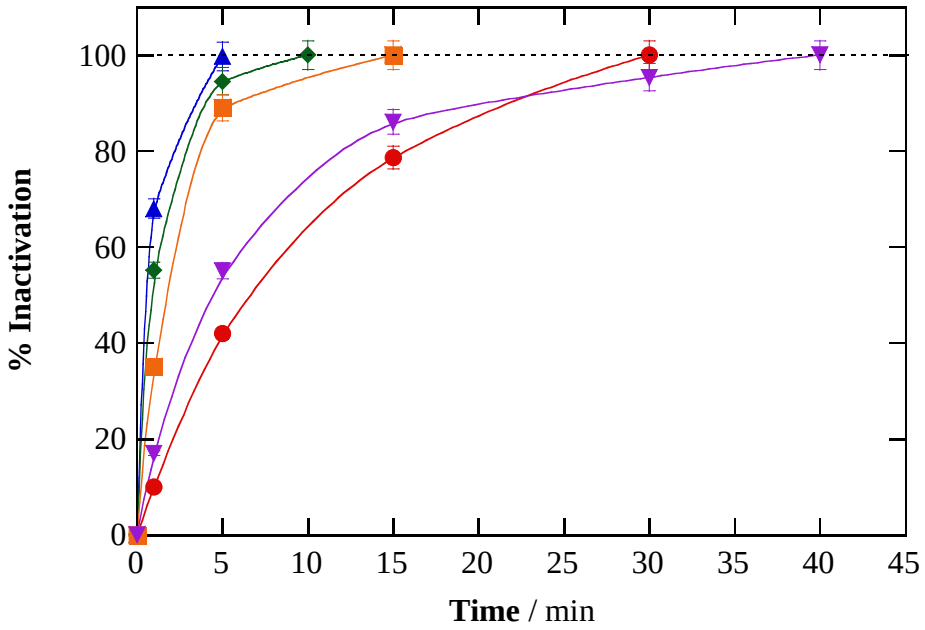

Fig. 1. Percentage of inactivation of 10^6 CFU mL^{-1} *Pseudomonas aeruginosa* aqueous suspensions with electrolysis time for the photoelectrocatalytic (PEC) treatment of 100 mL with (●) 7 mM and (▲,◆,■,▼) 25 mM Na_2SO_4 at pH 5.9 and 25 ºC. Trials were run in an undivided cell equipped with a 3 cm^2 photoanode illuminated with a 125 W UVA lamp and a stainless steel spiral as the cathode. Photoelectrode: (■) Ag(1%)-TiO_2 and (▼,◆,▲,●) Ag(4%)-TiO_2. Bias potential (E_{bias}): (◆) 1.00 and (■,▲,●) 1.70 V vs. Ag|AgCl (3 M KCl). In (▼), photocatalysis (PC) without the application of a bias potential.

This behavior can be related to the larger transfer of electrons from the VB of the TiO_2 nanoparticles, formed from reaction (1), to the more numerous Ag nanoparticles

263 [17,18]. Hence, the deposited Ag assists the external electric field to migrate the
264 photogenerated electrons from the TiO_2 film anode toward the counter electrode [46],
265 thus lowering the electron–hole recombination rates [47]. This phenomenon inhibits the
266 recombination of the generated holes with the e^-_{CB}, facilitating the production of a
267 larger amount of oxidant $^{\bullet}OH$ from reaction (2) and, finally, promoting the faster
268 inactivation of the microorganisms.

269 Fig. 1 also reveals a quicker inactivation when the Na_2SO_4 concentration rose from
270 7 (filled circle) to 25 mM (filled triangle) operating with the Ag(4%)-TiO_2 photoanode
271 at E_{bias} = 1.70 V. Up to 30 min were needed to completely inactivate the bacterium
272 when the lowest amount of electrolyte was employed, being 6-fold slower as compared
273 to PEC performed with 25 mM. This is due to the much higher *j* value circulating
274 through the photoelectrolytic cell because of the greater conductivity of the solution as
275 the supporting electrolyte content was increased. The upgrade of *j* then favors the
276 extraction of higher quantities of electrons accumulated in the Ag, which are transferred
277 from the VB of the TiO_2 by photoinduction. Consequently, the $^{\bullet}OH$ generation is
278 enhanced by the larger amount of holes available, thus accelerating the disinfection
279 process.

280 Another key parameter in PEC is the applied E_{bias} because it determines the ability
281 of the anode to extract the photoexcited electrons toward the cathode, controlling the *j*
282 value and the potential difference between the electrodes (E_{cell}). Fig. 1 reveals that using
283 the Ag(4%)-TiO_2 photoanode at E_{bias} = 1.00 V with 25 mM Na_2SO_4 (filled diamond),
284 the time for total inactivation was about 10 min, which is twice the value required at a
285 higher E_{bias} of 1.70 V (filled triangle). No greater inactivation rate was achieved by
286 further applying a higher E_{bias} of up to 2.00 V (data not shown). The higher *j* attained
287 upon gradual rise of E_{bias} up to 1.70 V favored the extraction of the photoinduced

288 electrons transferred to the Ag from the VB of the TiO_2. This led to a more rapid
289 inactivation of the *P. aeruginosa* cells thanks to the greater generation of $^{\bullet}OH$ from the
290 higher amount of holes formed in the TiO_2, as stated above.

291 The aforementioned findings indicate that, under the experimental conditions
292 tested, the best disinfection rate was achieved using a synthesized Ag(4%)-TiO_2 thin
293 film photoanode at the optimum E_{bias} = 1.70 V with 25 mM Na_2SO_4. These conditions
294 yielded a j = 0.8 mA cm^{-2} and E_{cell} = 5.0 V. The energy consumption for total
295 inactivation in 5 min was 104.18 kWh m^{-3}. This value mainly arises from the UVA
296 lamp consumption (104.17 kWh m^{-3}), since the energy requirements of the electrolytic
297 system only accounted for 0.01 kWh m^{-3}.

298 Several comparative PC trials were also performed to demonstrate the superior
299 disinfection power of PEC, as shown in Fig. 1. The gradual but slow inactivation of the
300 bacterium by PC under the best PEC conditions (Ag(4%)-TiO_2 photoanode in 25 mM
301 Na_2SO_4) required 40 min for the complete activity loss (upside-down filled triangle).
302 This entails a total energy consumption of 833.34 kWh m^{-3} for the PC treatment, a value
303 much greater than that determined for PEC at E_{bias} = 1.70 V, as pointed out above. This
304 result confirms the very important bactericidal role of the Ag particles added to the TiO_2
305 film in the PEC process, confirming its contribution to the minimization of the
306 recombination of the e^-_{CB}/h^+_{VB} pairs photogenerated in the semiconductor surface. This,
307 in concomitance with the application of an optimum E_{bias}, induces a much greater
308 production of $^{\bullet}OH$ from reaction (2). Note that the synthesized Ag(4%)-TiO_2
309 photocatalyst led to faster disinfection in PC as compared to the similar treatment of 10^8
310 CFU mL^{-1} of *P. aeruginosa* reported by Li et al. [36], since they needed 120 min for
311 achieving 99% inactivation of suspensions with 200 mg L^{-1} of Ag-TiO_2 microspheres.

The generation of •OH during the PEC treatment with an Ag(4%)-TiO_2 photoanode at E_{bias} = 1.70 V was confirmed by spin-trapping upon photoelectrolysis of a 9.2 mM DMPO solution with 25 mM Na_2SO_4 at pH 5.9 for 15 min. Fig. 2 presents the EPR spectrum found for the resulting solution, which clearly highlights the four characteristic bands (1:2:2:1) of the •OH-DMPO adduct. This corroborates the attack of •OH onto the outer layer of the *P. aeruginosa* in the above PEC trials, eventually inactivating the cells and probably causing their lysis.

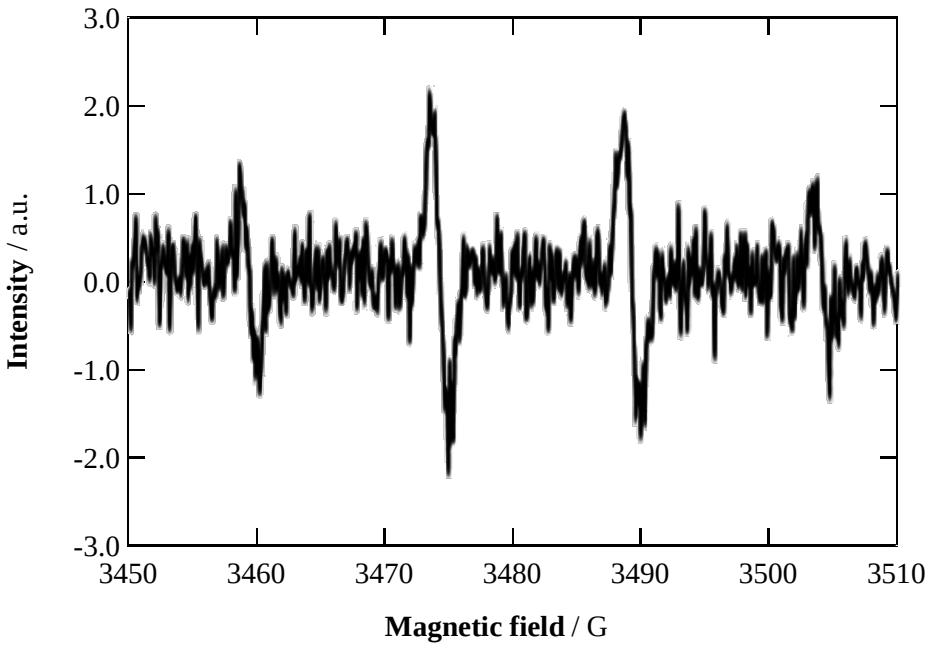

Fig. 2. EPR spectrum of the •OH-DMPO adduct detected in 10 mL of a 9.2 mM DMPO solution with 25 mM Na_2SO_4, at pH 5.9 and 25 ºC. The electrolysis was made using an Ag(4%)-TiO_2 photoanode illuminated with a 125 W UVA light and a stainless steel spiral cathode, both of 1 cm^2, at E_{bias} = 1.70 V vs. Ag|AgCl (3 M KCl) for 15 min.

3.2. Characterization of the synthesized Ag-TiO_2 photoanodes

The morphology of the Ag(4%)-TiO_2 film, the best photoanode synthesized for PEC in the present work, was assessed by HRTEM. Fig. 3a-c highlights the images obtained at increasing magnification, revealing the presence of non-spherical Ag and TiO_2 particles. These micrographs also suggest that the Ag nanoparticles are quite small but with a high degree of crystallinity. Fig. 3a clearly confirms the presence of cuboid-

shaped Ag in TiO_2 deposited powder. The P25 nanocrystals showed a size of about 100 nm. In Fig. 3b, the color contrast between gray TiO_2 and black Ag particles can be observed, being the average particle size of Ag nanoparticles around 45 nm.

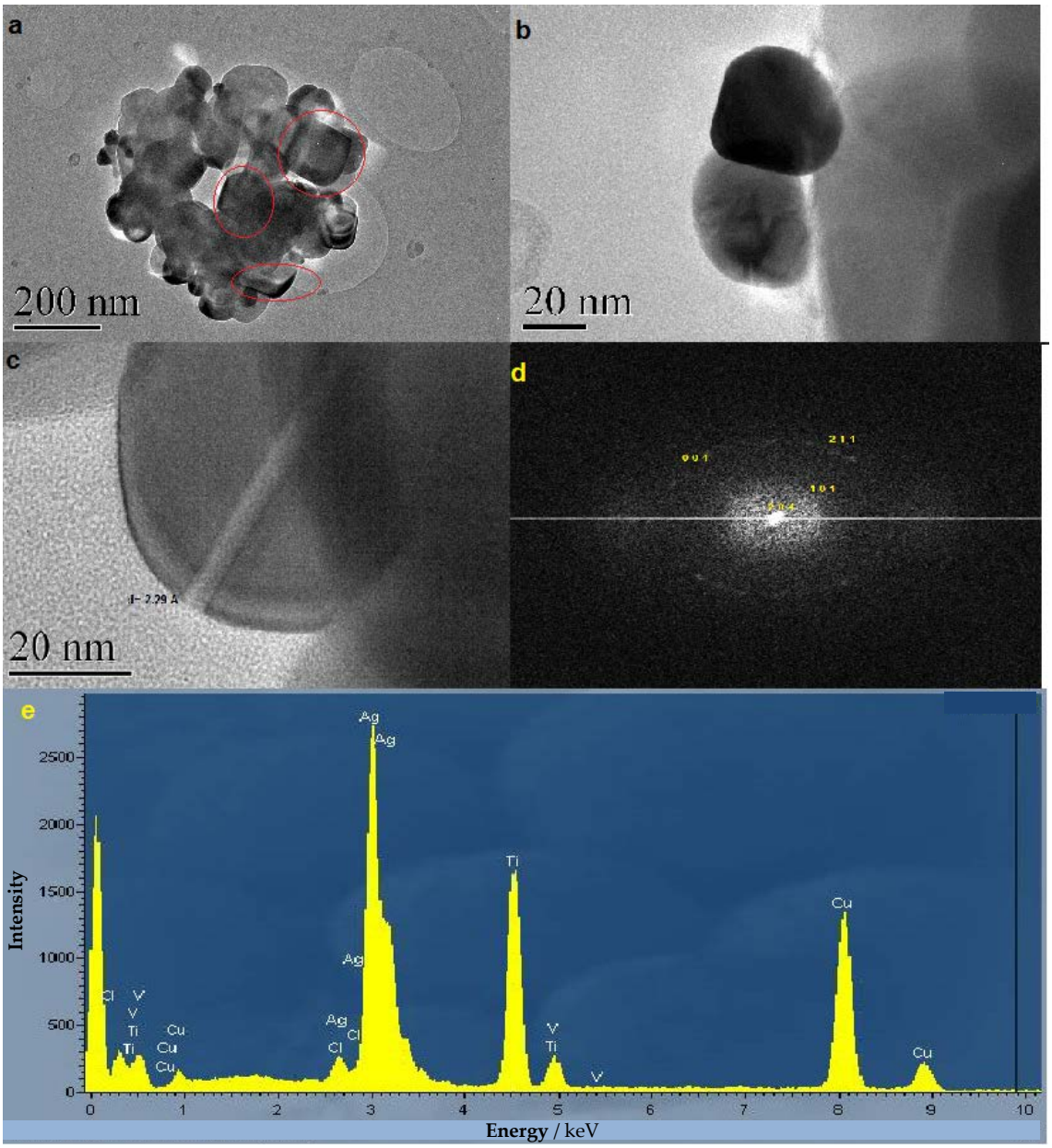

Fig. 3. HRTEM images of Ag(4%)-decorated TiO_2 powder, synthesized via electrophoresis method, at a magnification of (a) x20,000, (b) x150,000 and (c) x400,000. (d) SAED patterns of nano-TiO_2 powders revealing anatase or rutile phases. (e) EDX analysis of the Ag(4%)-TiO_2 sample shown in (c).

Fig. 3c shows the equal-thickness fringes of the anatase phase observed in a square-shape TiO_2 particle, indicating the presence of (101) facets with a lattice spacing of 2.29 Å. Selected area electron diffraction (SAED) patterns of nano-TiO_2 powders confirmed the predominance of anatase phase, as shown in Fig. 3d, where the ring pattern indicates the polycrystalline nature of TiO_2 nanoparticles. From the same diffraction pattern, it can be demonstrated that the ring consists of well distinct spots due to crystalline nature of TiO_2, which is an important prerequisite for the improvement of photocatalytic activity. The brightness and intensity of the polymorphic ring are quite weak, which can be related to a rather poor crystallinity with the presence of amorphous material. The observed (204), (004) and (211) planes agree with the standard data (JCPDS 75-1537) of TiO_2 anatase phase, whereas the (101) plane agrees with the standard data (JCPDS 88-1175) of TiO_2 rutile phase. The elemental composition of the photoanode was determined by EDX and the corresponding spectrum is shown in Fig. 3e. It evidences the pre-eminent presence of Ag and Ti with their characteristic peaks, along with those related to the Cu mesh and Cl or V impurities.

The crystalline planes of Ag and TiO_2 after annealing the electrode at 450 ºC were confirmed by XRD analysis. The diffractogram of Fig. 4 shows the peaks obtained for 2θ values between 10º and 80º, which can be ascribed to:

(i) The primary TiO_2 crystalline phase, i.e., anatase, with expected peaks at 25.2º, 37.3º, 47.6º, 53.5º, 55.1º and 62.2º for (101), (004), (200), (105), (211) and (204) planes (JCPDS Card No. 21-1272), respectively.

(ii) Rutile, with peaks at 27.3º, 35.6º, 41.2º, 54.3º and 67.2º corresponding to (110), (101), (111), (211) and (310) planes (JCPDS Card No. 21-1276), respectively.

(iii) Metallic silver, with peaks at 38.3º, 44.5º, 64.6º and 77.5º related to (111), (200), (220) and (311) planes (JCPDS Card No. 04-0783), respectively.

Undoped powder presented peaks at the same diffraction angles for both TiO_2 phases. Hence, it can be concluded that photodeposition of the silver does not modify the basic crystal structure of TiO_2, which can be related to a uniform decoration of the surface. Furthermore, it is noticeable that no peaks ascribed to AgO were found, meaning that Ag was only detected as pure metal, without oxides formation after annealing at 450 ºC.

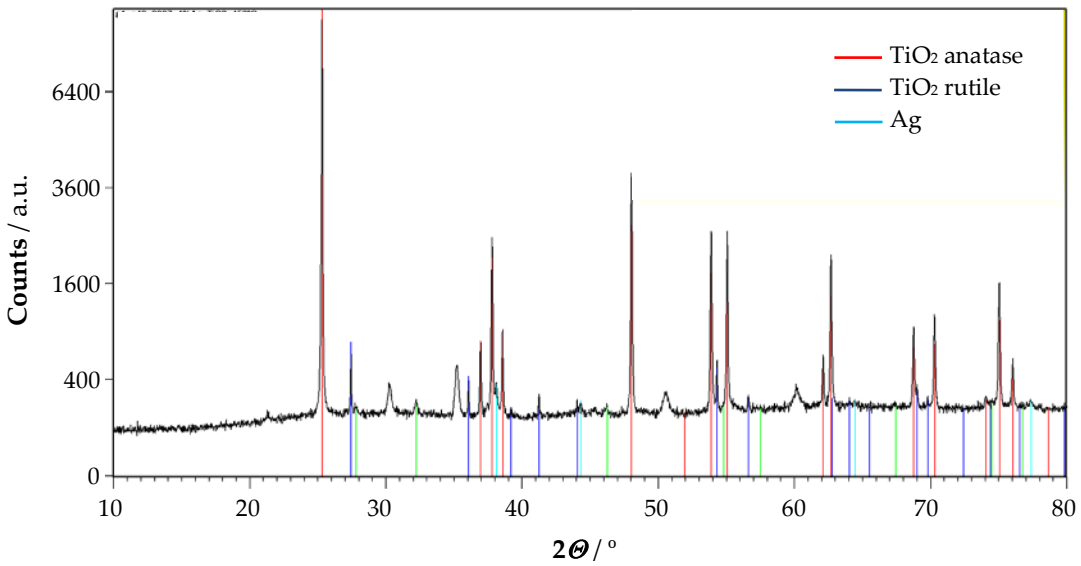

Fig. 4. XRD pattern of the ITO/Ag(4%)-TiO_2 photoanode after annealing at 450 ºC.

In addition, the optical properties of all materials were assessed from their UV/Vis absorption spectra, collected in Fig. 5. As can be seen, the ITO film did not absorb at any wavelength between 350 and 600 nm. In contrast, the TiO_2 deposited onto ITO absorbed the light in all the wavelength range checked, with higher intensity in the UV region up to near λ = 375 nm, whereupon the absorbance decreased very slowly within the visible region. The high absorption in the near-visible region is ascribed to the electron transition from VB to the CB, with an E_{bg} of 3.0-3.2 eV. The same behavior can be observed for the two synthesized Ag coating TiO_2 deposits, although with larger absorption in the visible region as the Ag content in the photocatalyst was increased, being accompanied by a shift to a higher λ where the visible absorption begins. The

higher absorbance in the visible region occurred from near λ = 405 nm for Ag(4%)-TiO_2, with a maximum shoulder at λ ~ 490 nm, thereby demonstrating its higher ability to absorb the visible light as compared to the other materials. Therefore, this is due to the enhanced photoexcitation of the electrons from the VB of the TiO_2 to the optimized number of Ag nanoparticles [48,49].

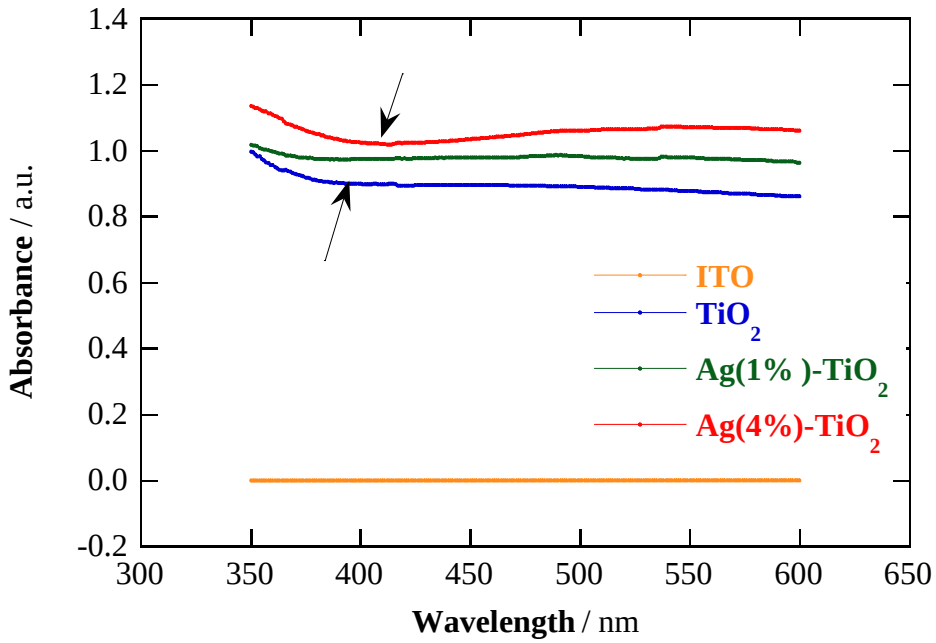

Fig. 5. UV-Vis absorption spectra of ITO, ITO/TiO_2 and ITO/Ag(4%)-TiO_2 after annealing at 450 ºC.

3.3. Comparative inactivation of Bacillus atrophaeus

The results of Fig. 1 demonstrate the effective attack of •OH produced at the Ag(4%)-TiO_2 photoanode onto the outer layer of *P. aeruginosa* bacteria. This layer is composed of peptidoglycans, consisting of a glycan backbone of muramic acid and glucosamine partially cross-linked with peptide chains. To clarify and extend the disinfection power of the PEC treatments tested, the process was also applied to the inactivation of a ubiquitous rod-shaped Gram-positive bacterium like *B. atrophaeus*. In this microorganism, the cell wall is more compact because it contains a densely crosslinked structure of peptidoglycans.

Fig. 6 evidences that a suspension with 10^6 CFU mL^{-1} of *B. atrophaeus* and 25 mM Na_2SO_4 can be completely disinfected after 15 min of PEC with an Ag(4%)-TiO_2 thin film photoelectrode at E_{bias} = 1.70 V. This time is much longer than 5 min required for the total inactivation of *P. aeruginosa* under comparable conditions (see Fig. 1). This finding agrees with the less compact outer layer of the Gram-negative bacterium, which can be more easily destroyed by •OH. The trend previously reported by us for the inactivation of 10^6 CFU mL^{-1} suspensions of both bacteria in Na_2SO_4 at pH 7.0 by means of EO with a BDD anode at j = 33.3 mA cm^{-2} was not so clear, since *B. atrophaeus* was very sensitive to significant pH variations at such high j [12].

The above results allow inferring that the synthesized Ag(4%)-TiO_2 photoanode can be useful for the fast and total disinfection of water contaminated with both, Gram-negative and Gram-positive bacteria, by means of PEC.

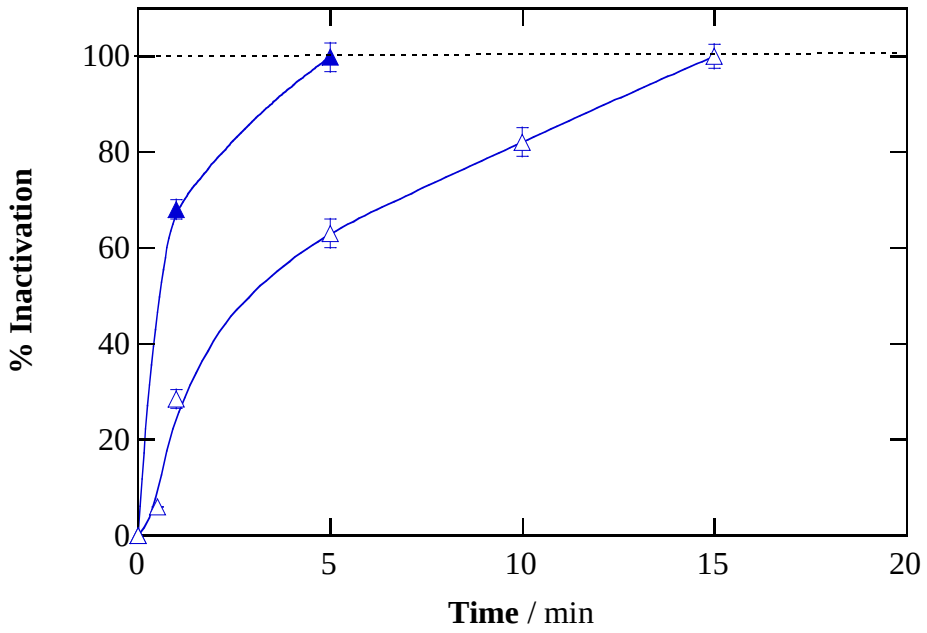

Fig. 6. Percentage of inactivation of 10^6 CFU mL^{-1} of (▲) *Pseudomonas aeruginosa* and (△) *Bacillus atrophaeus* aqueous suspensions *vs.* electrolysis time for the PEC treatment of 100 mL with 25 mM Na_2SO_4, at pH 5.9 and 25 ºC. Trials were made using an undivided cell with a 3 cm^2 Ag(4%)-TiO_2 photoanode illuminated with a 125 W UVA lamp at E_{bias} = 1.70 V vs. Ag|AgCl (3 M KCl).

3.4. Changes in bacterial morphology upon PEC treatment

Fig. 7a and b and Fig. 8a and b show the morphological features of the two bacteria prior to carrying out the PEC treatments, as obtained by SEM. As expected, a rod-shaped morphology with length of about 1-2 μm can be observed for both cell types.

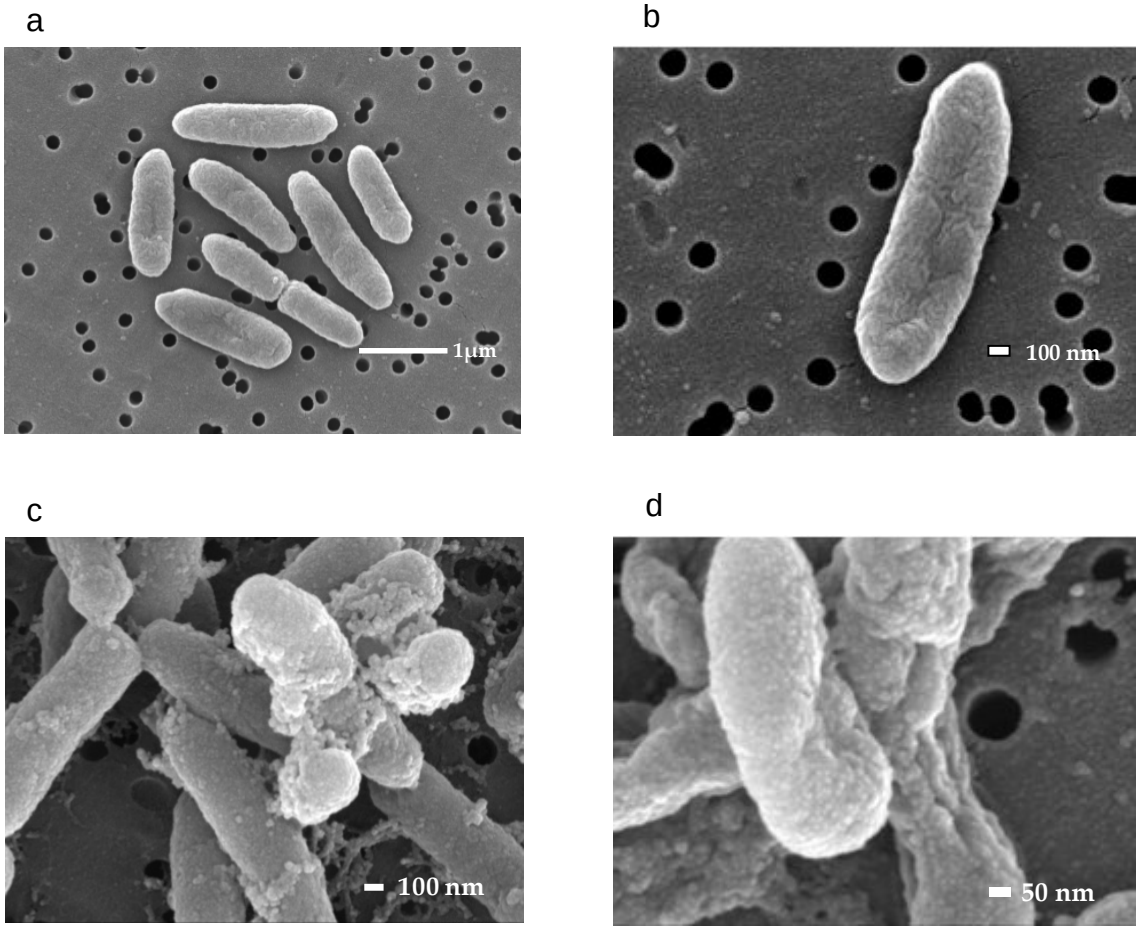

Fig. 7. SEM images for *Pseudomonas aeruginosa* supported on a polycarbonate membrane, corresponding to the assays of Fig. 6. (a, b) Initial suspension and (c, d) after 5 min of PEC. Magnification: (a) x20,000, (b, c) x40,000 and (d) x80,000.

Worth noting, the micrographs recorded after the total photoelectrocatalytic inactivation, at 5 min for *P. aeruginosa* (Fig. 7c and d) and at 15 min for *B. atrophaeus* (Fig. 8c and d), did not present significant alterations in their overall form and size, although their external surface became much rougher. In addition to such surface alteration, some cells were lysed and, consequently, cellular debris was accumulated in

the suspensions. This confirms the oxidation of some molecules of both cell walls by $^{\bullet}OH$, eventually weakening the structure. In conclusion, the inactivation can be accounted for by two phenomena promoted by the presence of such weaker wall: (i) the molecules within the cytoplasm are more exposed to external conditions, altering the cell metabolism, and (ii) collapse of the wall architecture that ends in the cell lysis with release of cytoplasmic material.

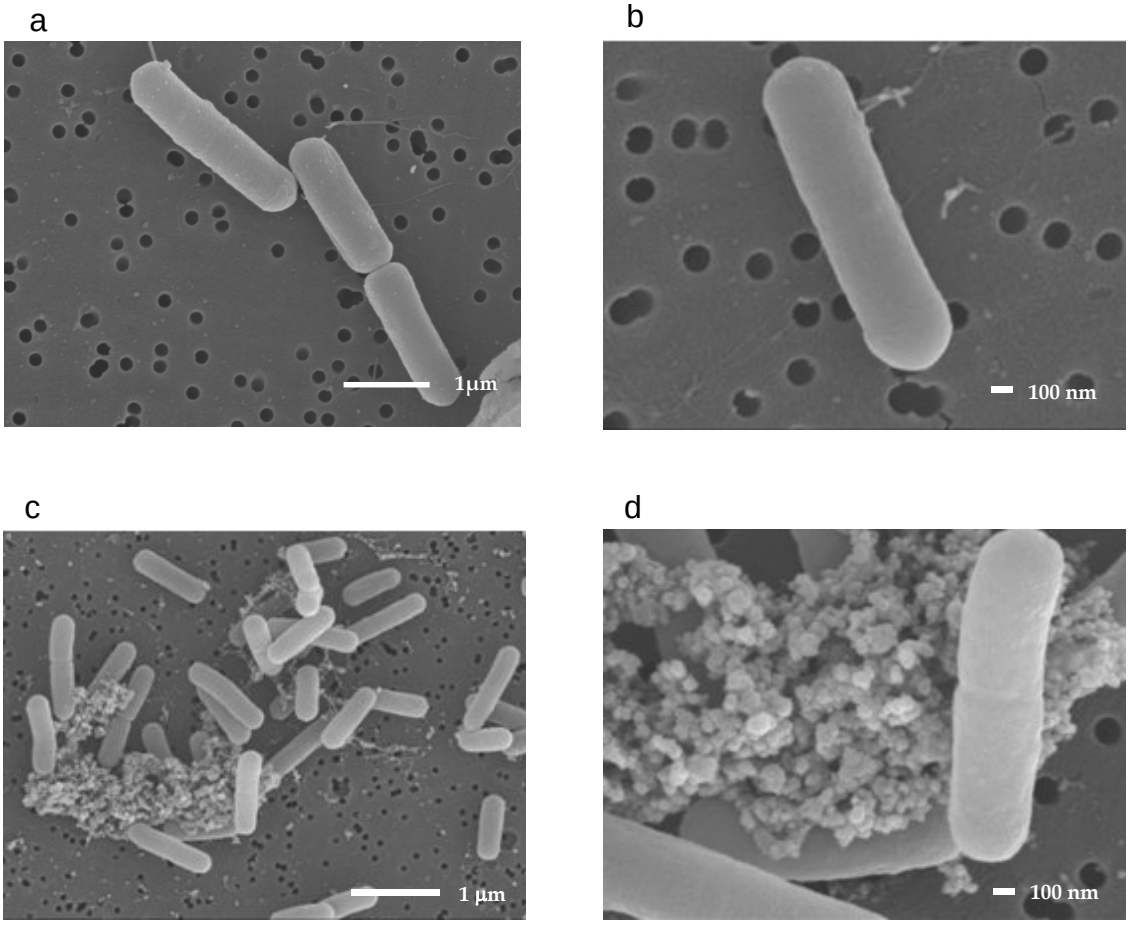

Fig. 8. SEM images for *Bacillus atrophaeus* supported on a polycarbonate membrane, corresponding to the assays of Fig. 6. (a, b) Initial suspension and (c, d) after 15 min of PEC. Magnification: (a, c) x10,000 and (b, d) x40,000.

4. Conclusions

It has been shown that *P. aeruginosa* suspensions at natural pH 5.9 can be rapidly disinfected by PEC using an Ag-TiO_2 thin film photoanode under UVA illumination.

497 The optimum experimental conditions were found with 4 wt.% Ag, in 25 mM Na_2SO_4
498 as supporting electrolyte and applying an E_{bias} = 1.70 V, which yielded complete
499 inhibition of this Gram-negative bacterium at a very short time of 5 min. The
500 comparative PC treatment required up to 30 min. This suggests the positive bactericidal
501 action of the photoanode under current supply in PEC, minimizing the recombination of
502 the photoinduced electron/hole pairs and upgrading the $^{\bullet}OH$ production, whose
503 presence was confirmed by EPR. The analysis of the synthesized Ag(4%)-TiO_2 revealed
504 that the photoanode was mainly composed of Ag nanoparticles on crystalline anatase,
505 and it possessed greater absorption in the visible region as compared to the unmodified
506 TiO_2 film. The PEC process was also useful to inactivate the Gram-positive bacterium
507 *B. atrophaeus*, which was more resistant due to its different cell wall formed by a thick
508 outer peptidoglycan layer.

509 **Acknowledgements**

510 The authors wish to thank financial support from project CTQ2016-78616-R
511 (AEI/FEDER, EU) and the National Council for Science and Technology (CONACyT)
512 of Mexico for the research grant to R.B. Domínguez-Espíndola.

513 **References**

514 [1] C.A. Martínez-Huitle, E. Brillas, Electrochemical alternatives for drinking water
515 disinfection, Angew. Chem. Int. Ed. 47 (2008) 1998-2005.
516 [2] M. Panizza, G. Cerisola, Direct and mediated anodic oxidation of organic
517 pollutants, Chem. Rev. 109 (2009) 6541-6569.

[3] I. Sirés, E. Brillas, M.A. Oturan, M.A. Rodrigo, M. Panizza, Electrochemical advanced oxidation processes: today and tomorrow. A review, Environ. Sci. Pollut. Res. 21 (2014) 8336-8367.

[4] E. Brillas C.A. Martínez-Huitle, Decontamination of wastewaters containing synthetic organic dyes by electrochemical methods. An updated review, Appl. Catal. B: Environ. 166-167 (2015) 603-643.

[5] C.A. Martínez-Huitle, M.A. Rodrigo, I. Sirés, O. Scialdone, Single and coupled electrochemical processes and reactors for the abatement of organic water pollutants: A critical review, Chem. Rev. 115 (2015) 13362-13407.

[6] F.C. Moreira, R.A.R. Boaventura, E. Brillas, V.J.P. Vilar, Electrochemical advanced oxidation processes: A review on their application to synthetic and real wastewaters, Appl. Catal. B: Environ. 202 (2017) 217-261.

[7] S. Cotillas, E. Lacasa, C. Sáez, P. Cañizares, M.A. Rodrigo, Disinfection of urine by conductive-diamond electrochemical oxidation, Appl. Catal. B: Environ. 229 (2018) 63-70.

[8] M. Zhou, M.A. Ouran, I. Sirés, Electro-Fenton Process: New Trends and Scale-Up, 1st ed., Springer, Singapore, 2018.

[9] S. Ghasemian, B. Asadishad, S. Omanovic, N. Tufenkji, Electrochemical disinfection of bacteria-laden water using antimony-doped tin-tungsten-oxide electrodes, Water Res. 126 (2017) 299-307.

[10] S.-C. Park, N.-H. Kim, W. Yang, J.-W. Nah, M.-K. Jang, D. Lee, Polymeric micellar nanoplatforms for Fenton reaction as a new class of antibacterial agents, J. Control. Release 221 (2016) 37-47.

[11] A. Nouri, M.T. Yaraki, M. Ghorbanpour, S. Agarwal, V.K. Gupta, Enhanced antibacterial effect of chitosan film using montmorillonite/CuO nanocomposite, Int. J. Biol. Macromol. 109 (2018) 1219-1231.

[12] C. Bruguera-Casamada, I. Sirés, M.J. Prieto, E. Brillas, R.M. Araujo, The ability of electrochemical oxidation with a BDD anode to inactivate Gram-negative and Gram-positive bacteria in low conductivity sulfate medium, Chemosphere 163 (2016) 516-524.

[13] E. Anfruns-Estrada, C. Bruguera-Casamada, H. Salvadó, E. Brillas, I. Sirés, R.M. Araujo, Inactivation of microbiota from urban wastewater by single and sequential electrocoagulation and electro-Fenton treatments, Water Res. 126 (2017) 450-459.

[14] Y. Zhang, X. Xiong, Y. Han, X. Zhang, F. Shen, S. Deng, H. Xiao, X. Yang, G. Yang, H. Peng, Photoelectrocatalytic degradation of recalcitrant organic pollutants using TiO_2 film electrodes: An overview, Chemosphere 88 (2012) 145-154.

[15] U.G. Akpan, B.H. Hameed, Parameters affecting the photocatalytic degradation of dyes using TiO_2-based photocatalysts: A review, J. Hazard. Mater. 170 (2009) 520-529.

[16] S. Garcia-Segura, E. Brillas, Applied photoelectrocatalysis on the degradation of organic pollutants in wastewaters, J. Photochem. Photobiol. C: Photochem. Rev. 31 (2017) 1-35.

[17] H. Zhang, G. Chen, D.W. Bahnemann, Environmental photo(electro)catalysis: fundamental principles and applied catalysts, in: G. Chen, C. Comninellis (Eds.), Electrochemistry for the Environmnent, Chapter 16, Springer, New York, 2010.

565 [18] M. Pelaez, N.T. Nolan, S.C. Pillai, M.K. Seery, P. Falaras, A. Kontos, P.S.M.
566 Dunlop, J.W.J. Hamilton, J.A. Byrne, K. O'Shea, M.H. Entezari, D.D. Dionysiou,
567 A review on the visible light active titanium dioxide photocatalysts for
568 environmental applications, Appl. Catal. B: Environ. 125 (2012) 331-349.
569 [19] J. Marugán, P. Christensen, T. Egerton, H. Purnama, Synthesis, characterization
570 and activity of photocatalytic sol-gel TiO_2 powders and electrodes, Appl. Catal. B:
571 Environ. 89 (2009) 273-283.
572 [20] V.V. Kondalkar, S.S. Mali, R.M. Mane, P.B. Dandge, S. Choudhury, C.K. Hong,
573 P.S. Patil, S.R. Patil, J.H. Kim, P.N. Bhosale, Photoelectrocatalysis of cefotaxime
574 using nanostructured TiO_2 photoanode: Identification of the degradation products
575 and determination of the toxicity level, Ind. Eng. Chem. Res. 53 (2014) 18152-
576 18162.
577 [21] J. Yu, M. Zhou, Effects of calcination temperature on microstructures and
578 photocatalytic activity of titanate nanotube films prepared by an EPD method,
579 Nanotechnology 19 (2008) 045606 (6 pp).
580 [22] K. Esquivel, L.G. Arriaga, F.J. Rodríguez, L. Martínez, L.A. Godínez,
581 Development of a TiO_2 modified optical fiber electrode and its incorporation into
582 a photoelectrochemical reactor for wastewater treatment, Water Res. 43 (2009)
583 3593-3603.
584 [23] C.-F. Liu, C.P. Huang, C.-C. Hu, Y. Juang, C. Huang, Photoelectrochemical
585 degradation of dye wastewater on TiO_2-coated titanium electrode prepared by
586 electrophoretic deposition, Separ. Purif. Technol. 165 (2016) 145-153.
587 [24] K Shankar, J.I. Basham, N.K. Allam, O.K. Varghese, G.K. Mor, X. Feng, M.
588 Paulose, J.A. Seabold, K.-S. Choi, C.A. Grimes, Recent advances in the use of

589 TiO_2 nanotube and nanowire arrays for oxidative photoelectrochemistry, J. Phys.
590 Chem. C 113 (2009) 6327-6359.
591 [25] Z. Han, L. Ren, Z. Cui, C. Chen, H. Pan, J. Chen, Ag/ZnO flower heterostructures
592 as a visible-light driven photocatalyst via surface plasmon resonance, Appl. Catal.
593 B: Environ. 126 (2012) 298-305.
594 [26] V.K. Sharma, R.A. Yngard, Y. Lin, Silver nanoparticles: green synthesis and their
595 antimicrobial activities, Adv. Colloid Interface Sci. 145 (2009) 83-96.
596 [27] X. Wang, X. Hou, W. Luan, D. Li, K. Yao, The antibacterial and hydrophilic
597 properties of silver-doped TiO_2 thin films using sol-gel method, Appl. Surf. Sci.
598 258 (2012) 8241-8246.
599 [28] M.F. Brugnera, M. Miyata, G.J. Zocolo, C.Q.F. Leite, M.V.B. Zanoni,
600 Inactivation and disposal of by-products from *Mycobacterium smegmatis* by
601 photoelectrocatalytic oxidation using Ti/TiO_2-Ag nanotube electrodes,
602 Electrochim. Acta 85 (2012) 33-41.
603 [29] K. Chen, X. Feng, R. Hu, Y. Li, K. Xie, Y. Li, H. Gu, Effect of Ag nanoparticle
604 size on the photoelectrochemical properties of Ag decorated TiO_2 nanotube
605 arrays, J. Alloys Comp. 554 (2013) 72-79.
606 [30] M.V. Sofianou, N. Boukos, T. Vaimakis, C. Trapalis, Decoration of TiO_2 anatase
607 nanoplates with silver nanoparticles on the {1 0 1} crystal facets and their
608 photocatalytic behaviour, Appl. Catal. B: Environ. 158-159 (2014) 91-95.
609 [31] A. Hernández-Gordillo, V. Rodríguez González, Silver nanoparticles loaded on
610 Cu-doped TiO_2 for the effective reduction of nitro-aromatic contaminants, Chem.
611 Eng. J. 261 (2015) 53-59.

612 [32] Y. Liu, S. Wei, W. Gao, Ag/ZnO heterostructures and their photocatalytic activity
613 under visible light: Effect of reducing medium, J. Hazard. Mater. 287 (2015) 59-
614 68.
615 [33] P.V.R.K. Ramacharyulu, J. Praveen Kumar, G.K. Prasad, A.R. Srivastava,
616 Synthesis, characterization and photocatalytic activity of Ag–TiO_2 nanoparticulate
617 film, RSC Adv. 5 (2015) 1309-1314.
618 [34] A. Shet, K.V. Shetty, Photocatalytic degradation of phenol using Ag core-TiO_2
619 shell (Ag@TiO_2) nanoparticles under UV light irradiation, Environ. Sci. Pollut.
620 Res. 23 (2016) 20055-20064.
621 [35] A. Shet, K.V. Shetty, Solar light mediated photocatalytic degradation of phenol
622 using Ag core - TiO_2 shell (Ag@TiO_2) nanoparticles in batch and fluidized bed
623 reactor, Solar Energy 127 (2016) 67-78.
624 [36] Y. Li, H. Ding, K. Mao, D. Wang, Q. Wang, W. Zhang, Bactericidal activity of
625 Ag nanoparticles decorated TiO_2 microspheres and effects of water composition
626 and extracellular polymeric substances, Clean 43 (2015) 512–520.
627 [37] S. Malato, M.I. Maldonado, P. Fernández-Ibáñez, I. Oller, I. Polo, R. Sánchez-
628 Moreno, Decontamination and disinfection of water by solar photocatalysis: The
629 pilot plants of the Plataforma Solar de Almeria, Mater. Sci. Semiconductor
630 Process. 42 (2016) 15-23.
631 [38] P.V.L. Reddy, B. Kavitha, P.A.K. Reddy, K.-H. Kim, TiO_2-based photocatalytic
632 disinfection of microbes in aqueous media: A review, Environ. Res. 154 (2017)
633 296-303.
634 [39] A.B.K. dos Santos, E.M.T. Claro, R.N. Montagnolli, J.M. Cruz, P.R.M. Lopes,
635 E.D. Bidoia, Electrochemically assisted photocatalysis: Highly efficient treatment

using thermal titanium oxides doped and non-doped electrodes for water disinfection, J. Environ. Manage. 204 (2017) 255-263.

[40] M.F. Brugnera, M. Miyata, G.J. Zocolo, C.Q.F. Leite, M.V.B. Zanoni, A photoelectrocatalytic process that disinfects water contaminated with *Mycobacterium kansasii* and *Mycobacterium avium*, Water Res. 47 (2013) 6596-6605.

[41] K.D. Mena, C.P. Gerba, Risk assessment of *Pseudomonas aeruginosa* in water, Rev. Environ. Contam. Toxicol. 201 (2009) 71-115.

[42] S.N. Hussain, A.P. Trzcinski, H.M.A. Asghar, H. Sattar, N.W. Brown, E.P.L. Roberts, Disinfection performance of adsorption using graphite adsorbent coupled with electrochemical regeneration for various microorganisms present in water, J. Ind. Eng. Chem. 44 (2016) 216-225.

[43] T.H.R. Niepa, L.M. Snepenger, H. Wang, S. Sivan, J.L. Gilbert, M.B. Jones, D. Ren, Sensitizing *Pseudomonas aeruginosa* to antibiotics by electrochemical disruption of membrane functions, Biomaterials 74 (2016) 267-279.

[44] C. Bruguera-Casamada, I. Sirés, E. Brillas, R.M. Araujo, Effect of electrogenerated hydroxyl radicals, active chlorine and organic matter on the electrochemical inactivation of *Pseudomonas aeruginosa* using BDD and dimensionally stable anodes, Separ. Purif. Technol. 178 (2017) 224-231.

[45] B. Borbón, M.T. Oropeza-Guzman, E. Brillas, I. Sirés, Sequential electrochemical treatment of dairy wastewater using aluminium and DSA-type anodes, Environ. Sci. Pollut. Res. 21 (2014) 8573-8584.

[46] C. He, Y. Xiong, J. Chen, C. Zha, X. Zhu, Photoelectrochemical performance of Ag–TiO_2/ITO film and photoelectrocatalytic activity towards the oxidation of organic pollutants, J. Photoch. Photobio. A. 157 (2003) 71-79.

661 [47] A. Zielińska, E. Kowalska, J.W. Sobczak, I. Łacka, M. Gazda, B. Ohtani, J. Hupka,
662 A. Zaleska, Silver-doped TiO_2 prepared by microemulsion method: surface
663 properties, bio-and photoactivity, Sep. Purif. Technol. 72 (2010) 309-318.
664 [48] C.A. Castro, P. Osorio, A. Sienkiewicz, C. Pulgarin, A. Centeno, S.A. Giraldo,
665 Photocatalytic production of $^1O_2$ and $^{\bullet}OH$ mediated by silver oxidation during the
666 photoinactivation of *Escherichia coli* with TiO_2, J. Hazard. Mater. 211-212 (2012)
667 172-181.
668 [49] D. Kong, J.Z.Y. Tan, F. Yang, J. Zeng, X. Zhang, Electrodeposited Ag
669 nanoparticles on TiO_2 nanorods for enhanced UV visible light photoreduction
670 CO_2 to CH_4, Appl. Surf. Sci. 277 (2013) 105-110.